Efficient conversion from infrared to red light by cascaded nonlinear optical processes using an aperiodically poled lithium niobate crystal

Juan Eduardo González [a], Luis Antonio Ríos [a], Diego Rubén Yankelevich [b], Roger Sean Cudney [a,*]

[a] *Departamento de Óptica, Centro de Investigación Científica y de Educación Superior de Ensenada, Carretera Ensenada-Tijuana No. 3918, Zona Playitas, Ensenada, B.C. CP 22860, Mexico*
[b] *Department of Electrical and Computer Engineering, University of California, 3101 Kemper Hall, Davis, CA 95616, USA*

Abstract

We present a scheme for conversion of pulsed light from the infrared to the red spectral region, using an aperiodically poled ferroelectric crystal within a resonant cavity in which two cascaded nonlinear optical processes occur when pumped with a pulsed Nd:YAG laser. This device emits 9 ns pulses of over 1 mJ at 710 nm and is a viable source for future biomedical applications.

All Rights Reserved © 2015 Universidad Nacional Autónoma de México, Centro de Ciencias Aplicadas y Desarrollo Tecnológico. This is an open access item distributed under the Creative Commons CC License BY-NC-ND 4.0.

Keywords: Lithium niobate; Nonlinear wave mixing; Nonlinear optics; Devices; Parametric oscillators and amplifiers

Lasers have a wide range of applications in medicine, both in surgery and diagnostics, mainly since they can be made to interact with selected target area regions with minimal collateral damage to nearby regions. Some of these biomedical applications require the use of light in the red and near infrared region of the spectrum; for example the ruby laser has been used successfully in treatment of melanoma (Polla et al., 1987), destruction of hair follicles (Grossman, Dierickx, Farinelli, Flotte, & Anderson, 1996) and tattoo removal (Goldman, Wilson, Hornby, & Meyer, 1965) among other applications. The HeNe laser has also been used successfully for capillary blood flow measurement using the technique of laser-Doppler spectroscopy (De Mul et al., 1984) and also in dermatology for the treatment of skin spots or to stimulate tissue regeneration in scars.

Photoacoustic imaging, also called optoacoustic imaging, is a diagnostic technique which is based on the detection of acoustic waves induced in tissue by the absorption of electromagnetic radiation, usually from pulsed sources on a nanosecond timescale. The optical wavelengths most commonly used are between 600 and 900 nm because they can penetrate up to several centimeters of human tissue (Emelianov et al., 2006). This technique can be used to detect hemoglobin, lipids, water, microcalcifications in breast tissue, among other things. In the particular case of microcalcifications, a wavelength between 600 and 800 nm is optimal to obtain photoacoustic images (Kang et al., 2011); however the optical pulse sources currently used for this technique are expensive and bulky, which restricts the further application of this technology in medicine and biology.

As an alternative to the current light sources, in recent works the use of optical parametric oscillators (OPO) based on aperiodically poled ferroelectric crystals has been proposed. In these devices light in the red spectral region can be obtained through nonlinear optical processes, for example in (Figen & Akın, 2014) a device was presented that emits at 632 nm using a Nd:YAG laser as the pump source, with the OPO being injection-seeded with a 1550 nm laser diode.

Here we present a simple device that emits nanosecond pulses at a wavelength of 710 nm (deep red) specifically for photoacoustic imaging which is also based on an aperiodically poled ferroelectric crystal. In this case however, it requires only a Nd:YAG laser source to obtain the red beam.

---

* Corresponding author.

E-mail address: rcudney@cicese.mx (R.S. Cudney).

Peer Review under the responsibility of Universidad Nacional Autónoma de México.

We convert light from 1064 nm to 710 nm with quasi-phase-matching obtained with an aperiodically poled lithium niobate crystal, as described in (Robles-Agudo & Cudney, 2011). In order to achieve this conversion it is necessary to perform at least two cascaded nonlinear optical processes within the crystal. We designed a crystal which produces optical parametric generation at the degeneracy point, i.e. the signal and idler wavelengths are the same, 2128 nm, which is twice the wavelength of the pump beam, and simultaneously a sum-frequency generation process between the pump and signal waves resulting in a beam with a wavelength equal to 2/3 of the pump wavelength, 710 nm.

From Maxwell's equations we can deduce the coupling among the waves. Let A_p, A_s and A_r be the electric field amplitudes of the pump, signal and red waves, with angular frequencies of ω_p, ω_s and ω_r, and k_p, k_s and k_r their corresponding wavevectors. Assuming that the three waves are co-propagating along the same direction, from Maxwell's equations we deduce that the coupled wave equations for these amplitudes are

$$\frac{d}{dz}A_s = i\frac{\omega_s}{2n_s c}\chi^{(2)}(z)(2A_p A_s^* e^{i\Delta k_{OPO}z} + A_r A_p^* e^{i\Delta k_{SFG}z}), \quad (1)$$

$$\frac{d}{dz}A_p = i\frac{\omega_p}{2n_p c}\chi^{(2)}(z)(A_s^2 e^{-i\Delta k_{OPO}z} + A_r A_s^* e^{i\Delta k_{SFG}z}), \quad (2)$$

$$\frac{d}{dz}A_r = i\frac{\omega_r}{2n_r c}\chi^{(2)}(z)A_s A_p e^{-i\Delta k_{SFG}z}. \quad (3)$$

Here z is the distance along the propagation direction of the waves, n_p, n_s and n_r are the refractive indices of the pump, signal and red waves, $\chi^{(2)}(z)$ is the spatially-varying nonlinearity of the medium, c is the speed of light and Δk_{OPO} and Δk_{SFG} are the propagation constant mismatches of the optical parametric and sum-frequency generation processes, given by

$$\Delta k_{OPO} = k_p - 2k_s, \quad (4)$$

$$\Delta k_{SFG} = k_r - k_s - k_p. \quad (5)$$

Since the magnitudes of the wavevectors are given by $k = \omega n/c$ and since the refractive index depends on the angular frequency ω, the propagation constant mismatches are non-zero; this limits the coupling of the fields and ultimately the conversion efficiency into the red beam. To increase the coupling efficiency, the complex exponential factors appearing in Eqs. (1)–(3) must be compensated by the spatially varying nonlinearity, that is, $\chi^{(2)}(z)$ must have a non-negligible Fourier component for both processes, given by (Robles-Agudo & Cudney, 2011)

$$\chi^{(2)}(\Delta k_j) = \int_0^L \chi^{(2)}(z)e^{i\Delta k_j z}dz, \quad (6)$$

where L is the length of the nonlinear medium. However, in order to generate the red beam the signal beam must be generated first, so it is necessary to control the ratio of the magnitudes of each of the Fourier components. We accomplish this by creating an aperiodically poled LiNbO$_3$ crystal (APLN) that has the appropriate Fourier components (Kartaloğlu, Figen, & Aytür, 2003; Robles-Agudo & Cudney, 2011). We define

$$g(z) = sgn[(1-w)\cos(\Delta k_{OPO}z) + w\cos(\Delta k_{SFG}z)], \quad (7)$$
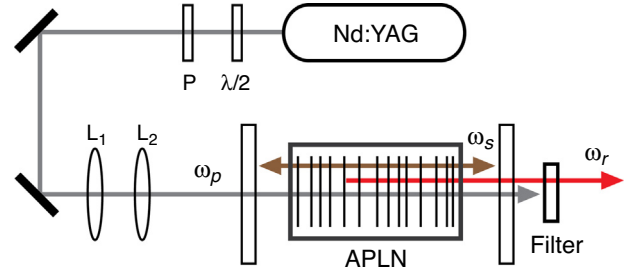

Figure 1. Experimental setup.

where w is a weighting parameter used to adjust the contribution of each of the Fourier components. From this function we design the APLN: we create a domain structure that follows $g(z)$. If all of the waves have extraordinary polarization then $\chi^{(2)}(z) = \chi_{33}^{(2)}g(z)$.

We designed several domain structures with different values of w. Using the refractive indices predicted by the Sellmeier equation given in (Jundt, 1997), we calculate that $k_{OPO} = 0.198 \,\mu m^{-1}$ and $k_{SFG} = 0.383 \,\mu m^{-1}$ (corresponding to periodicities of 31.8 and 16.4 μm), assuming operation at room temperature. These designs were transferred using standard photolithographic and electrical poling techniques (Cudney, Ríos, Arellanes, Alonso, & Fonseca, 2002) onto a 500 μm thick, z-cut LiNbO$_3$ wafer. After cutting and polishing, the crystal was 34 mm long, and antireflection coatings for 2.2 μm were deposited on the end facets. The crystal was placed in the experimental setup shown in Figure 1. As a pump we used a Nd:YAG laser that emits 12 ns long (FWHM) pulses with a repetition rate of 10 Hz. We used a half-wave plate ($\lambda/2$) and a Glan–Thompson polarizer (P) to vary the energy of the pump beam. In order to increase the conversion efficiency from the pump beam to the red beam, the APLN crystal was placed in a resonant cavity formed by two flat dielectric mirrors separated by 5.8 cm which are highly reflective at the signal wavelength and highly transmitting at both the pump and red wavelengths, i.e. we made an OPO that oscillates at $\lambda = 2128$ nm.

The maximum pump energy that can be used is determined by the damage threshold of the APLN crystal, which is approximately 3 J/cm^2. Since the APLN crystal is only 500 μm thick, the maximum pump energy that can be used without damaging the sample is around 6 mJ, assuming the beam has a circular cross section. In order to circumvent this restriction we focused the pump beam to an elliptical cross-section (0.34 mm × 2.8 mm, FWHM) by using a pair of lenses, a 400 mm focal length spherical lens (L$_1$) and a 100 mm focal length cylindrical lens (L$_2$).

We obtained a red beam with all of the domain structures; in all cases it had a spectrum centered at 710 nm with a large bandwidth (~10 nm FWHM) and a temporal duration of ~9 ns (FWHM) (Yankelevich, González, Cudney, Ríos, & Marcu, 2014). The output energy per pulse at 710 nm vs. pump energy for the best two structures, one with $w = 0.20$ and the other with $w = 0.34$, is shown in Figure 2.

As can be seen, in both cases the threshold to obtain the red beam is around 1 mJ. However, above the threshold the conversion efficiency is higher for $w = 0.34$. At a pump level of 7 mJ
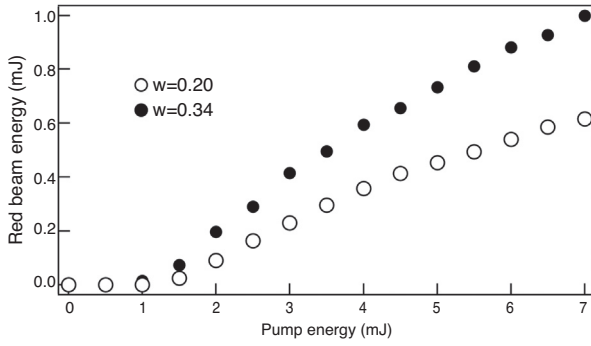
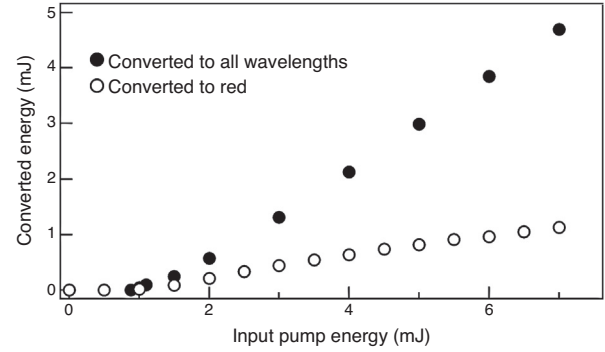Figure 2. Output energy of the red beam vs. pump energy.

Figure 4. Energy converted to other frequencies.

per pulse we obtain 1 mJ at 710 nm, i.e. we have an efficiency of more than 14%.

We also studied the time evolution of the pulses. The red and pump beams were separated with a diffraction grating and the pulses were detected by fast rise-time photodiodes (the temporal resolution was limited by the bandwidth of the oscilloscope, 1 GHz). The results are shown in Figure 3. Figure 3(a) shows the results obtained when the pump energy is just below the threshold; as can be expected, the red beam is not present. If the OPO is pumped above threshold, the red beam appears and the shape of the pump pulse at the output of the OPO is altered: the peak is depleted due to conversion of the pump into the signal and red beams, as shown in Figure 3(b) and (c). Finally, if the pump energy is several times the threshold, the pump beam is depleted but a secondary peak in the depletion zone appears, as shown in Figure 3(d). This is due to back conversion of the signal and red beams into the pump, which is indicative of a very high conversion of the pump into other wavelengths.

From the deformation of the pump pulse we can calculate how much of the pump is converted into other wavelengths. It can be readily shown that the fraction of the energy of the pump pulse that was not converted to other frequencies f_p is given by (Arellanes & Cudney, 2001)

$$f_p = \frac{\int_{-\infty}^{\infty} I_p dt}{\int_{-\infty}^{\infty} I_p^{th} dt} \cdot \frac{E_p^{th}}{E_p} \tag{8}$$

where E_p and I_p are the energy and the temporal profile of the pump pulse, and E_p^{th} and I_p^{th} are the energy and the temporal profile at the threshold. The fraction of the input energy that is converted to other frequencies is simply $1 - f_p$. Figure 4 shows the input energy converted to other wavelengths as a function of the input pump energy; for comparison, the energy of the red beam previously shown in Figure 2 is also shown. As can be seen, at 7 mJ input energy over 67% is converted into other wavelengths, mainly the 2.12 μm signal and the 710 nm red beams.
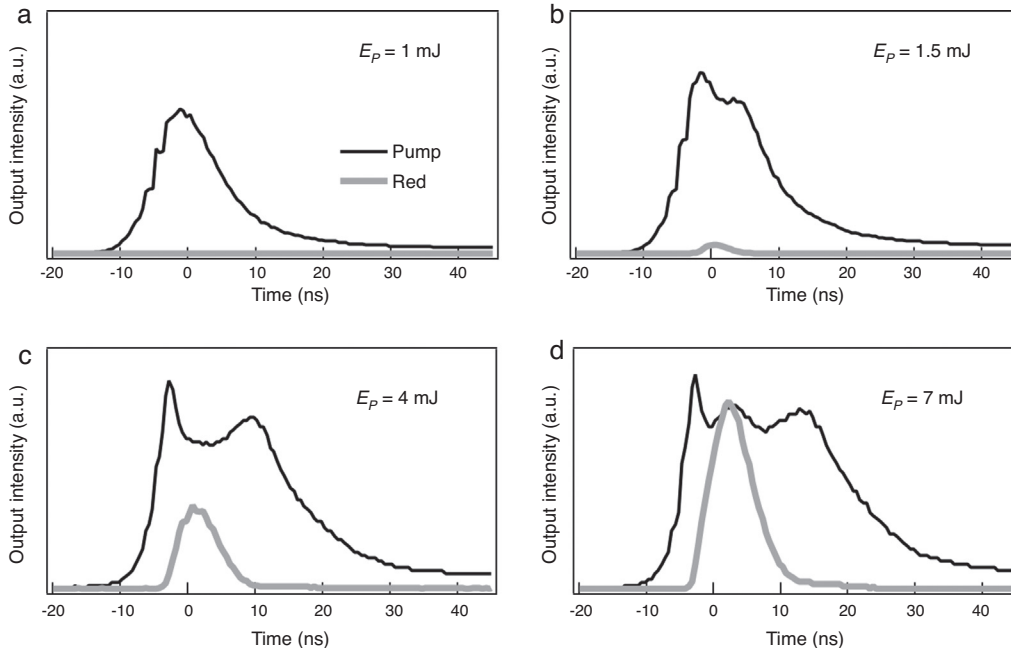

Figure 3. Temporal profiles of the output pump and red beams. (a) Just below threshold; (b) and (c): above threshold; (d) above threshold, back conversion into the pump is observed. Each curve is the result of the running average over 100 pulses.

In conclusion, we made a simple, inexpensive device that emits nanosecond pulses of broadband 710 nm radiation, based on cascaded optical parametric oscillation at the degeneracy point and sum-frequency generation in a single aperiodically poled lithium niobate crystal. We obtained more than 1 mJ of radiation at 710 nm with only 7 mJ of pump energy at 1.064 μm.

Conflict of interest

The authors have no conflicts of interest to declare.

Acknowledgements

References

Arellanes, M. O., & Cudney, R. S. (2001). Construcción y caracterización de un oscilador óptico paramétrico con niobato de litio periódicamente polarizado. *Revista Mexicana de Física*, *47*(5), 460–466.

Cudney, R. S., Ríos, L. A., Arellanes, M. O., Alonso, F., & Fonseca, J. (2002). Fabricación de niobato de litio periódicamente polarizado para óptica no lineal. *Revista Mexicana de Física*, *48*(6), 548–555.

De Mul, F. F. M., Van Spijker, J., Van der Plas, D., Greve, J., Aarnoudse, J. G., & Smits, T. M. (1984). Mini laser-Doppler (blood) flow monitor with diode laser source and detection integrated in the probe. *Applied Optics*, *23*(17), 2970–2973.

Emelianov, S.Y., Aglyamov, S.R., Karpiouk, A.B., Mallidi, S., Park, S., Sethuraman, S., Shah, J., Smalling, R.W., Rubin, J.M., & Scott, W.G. (2006). 1E-5 synergy and applications of combined ultrasound, elasticity, and photoacoustic imaging. *InUltrasonics Symposium*, 2006. *IEEE* (pp. 405–415). IEEE.

Figen, Z. G., & Akın, O. (2014). Red beam generation based on aperiodically poled lithium niobate. *Optics Communications*, *317*, 67–77.

Goldman, L., Wilson, R. G., Hornby, P., & Meyer, R. G. (1965). Radiation from a Q-switched ruby laser. *Journal of Investigative Dermatology*, *44*(1), 69–71.

Grossman, M. C., Dierickx, C., Farinelli, W., Flotte, T., & Anderson, R. R. (1996). Damage to hair follicles by normal-mode ruby laser pulses. *Journal of the American Academy of Dermatology*, *35*(6), 889–894.

Jundt, D. H. (1997). Temperature-dependent Sellmeier equation for the index of refraction, ne, in congruent lithium niobate. *Optics Letters*, *22*(20), 1553–1555.

Kang, J., Kim, E. K., Kwak, J. Y., Yoo, Y., Song, T. K., & Chang, J. H. (2011). Optimal laser wavelength for photoacoustic imaging of breast microcalcifications. *Applied Physics Letters*, *99*(15), 153702.

Kartaloğlu, T., Figen, Z. G., & Aytür, O. (2003). Simultaneous phase matching of optical parametric oscillation and second-harmonic generation in aperiodically poled lithium niobate. *Journal of the Optical Society of America B*, *20*, 343–350.

Polla, L. L., Margolis, R. J., Dover, J. S., Whitaker, D., Murphy, G. F., Jacques, S. L., et al. (1987). Melanosomes are a primary target of Q-switch ruby laser irradiation in guinea pig skin. *Journal of Investigative Dermatology*, *89*(3), 281–286.

Robles-Agudo, M., & Cudney, R. S. (2011). Multiple wavelength generation using aperiodically poled lithium niobate. *Applied Physics B*, *103*(1), 99–106.

Yankelevich, D., González, J. E., Cudney, R. S., Ríos, L. A., & Marcu, L. (2014). Development of a new pulsed source for photoacoustic imaging based on aperiodically poled lithium niobate. *Biomedical Optics Express*, *5*(2), 468–473.